Chapter 4

Contact model

The numerical method described in Chapter 3 computes the motion of a sphere and the evolution of the surrounding flow field before the sphere collides with a wall. To simulate the collision process, a contact model is required to capture the contact mechanism of an immersed collision process. In the beginning of this chapter, the physics of a lubricated impact of a steel sphere on a glass plate is introduced briefly. Then, a contact model is developed to deal with the two difficult points in numerical simulations, the thin lubrication layer effect and the elastic deformation of the solid parts. The liquid-solid interaction forces for a sphere moving in a viscous liquid with steady/unsteady velocity are briefly reviewed especially for the case when there is another solid boundary, such as a solid wall. Based on the analytical formulas that are presented and well proven by previous researchers, a liquid-solid interaction force is proposed to incorporate the lubrication effect when a sphere is close to a wall. The elasticity of the solid materials is incorporated by applying an elastic-like force on a sphere when the distance between the sphere and the wall diminishes below a threshold value. The new force term is defined based on Hertz elastic theory and includes the inelastic effect to dissipate the kinetic energy of the sphere during collision.

4.1 Physics of a lubricated impact of a sphere on a wall

People investigated the contact mechanism of a lubricated impact of a sphere on a wall by coupling the fluid dynamics and the elastic solid mechanics. The results of a steel ellipsoidal sphere impacting on a glass plate given by Al-Samieh & Rahnejat (2002) are represented in figure (4.1). The shape

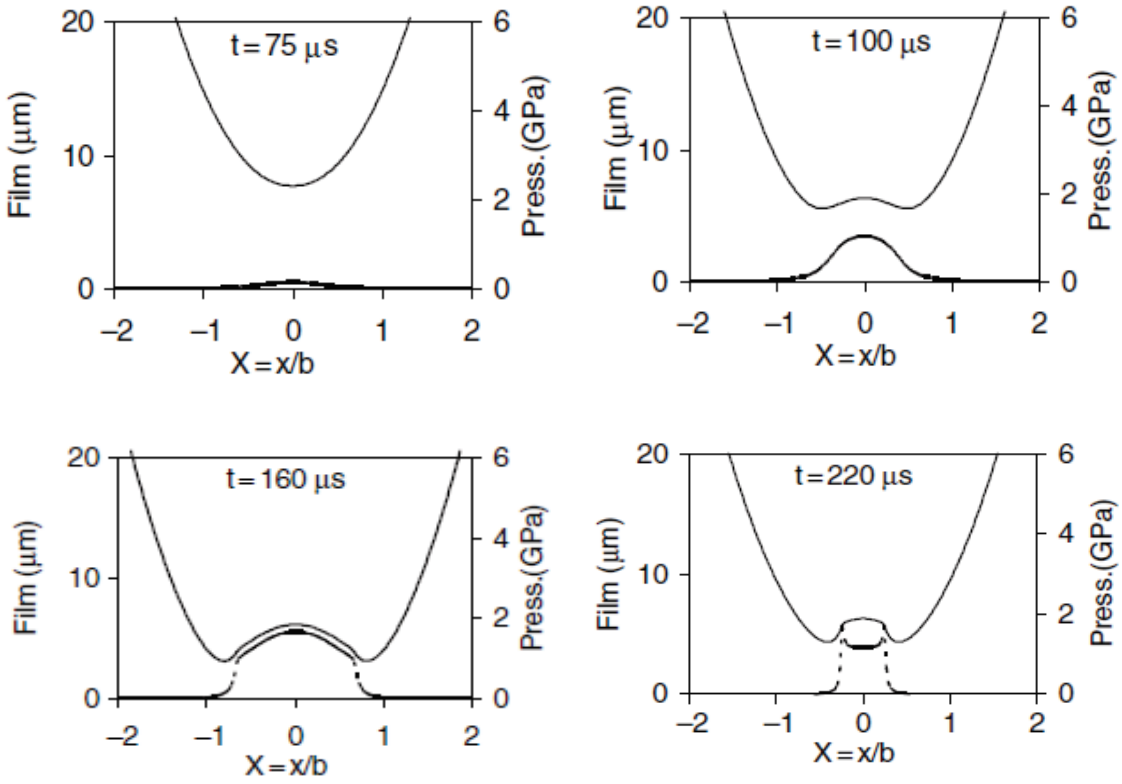

Figure 4.1: Physics of a lubricated impact of a sphere on a wall. The shape of the elastic sphere and the pressure distribution in the interstitial liquid layer are presented together at different time steps.

of the elastic sphere is presented together with the pressure distribution in the interstitial liquid layer. As the sphere approaches the plate, high pressure building up in the lubrication layer deforms the elastic body and makes the sphere rebound before it actually contacts the plate. This can be considered to be the essential physics during an immersed collision process.

As shown in figure (4.1), the liquid layer is very thin (about several micrometers) and hard to be resolved in a numerical simulation. Using a finer grid can delay but not prevent the problem. Also, the particle and wall are rigid in the current simulations; hence, the elasticity of the materials is not included. As a result, the simulations do not include the energy stored in the elastic deformation of the sphere and the wall, which is critical to the rebounding of an impacting sphere. To deal with those problems, a contact model is developed to capture the collision process: the effect of the liquid layer is incorporated by using a liquid-solid interaction force term; the elastic deformation of the solid parts is incorporated by using an elastic force term.

4.2 Liquid-solid interaction force with wall effect

The interaction between a moving solid particle and the surrounding fluid has been studied by different researchers. A thorough review can be found in Michaelide (1997). Three types of hydrodynamic forces are most widely discussed and established. The Stokes drag force is an expression for the force exerted on a sphere steadily moving in an unbounded viscous liquid. The unsteady forces due to acceleration of the relative velocity of a body can be divided into two parts: the added mass force and the history force. The added mass force accounts for the inertia added to a solid body because of an acceleration or deceleration relative to the fluid. The history force addresses the temporal delay of the boundary layer development when the relative velocity between the particle and the surrounding fluid varies in time. When there is an additional solid boundary, the hydrodynamics forces are influenced because the fluid is restricted by the second solid boundary. Prior studies have developed correction terms for the gap between the two solid boundaries on the three forces. Yang (2006) summarized and simplified the analytical formulas for the hydrodynamic forces including the wall effect and validated the formulas with experimental results. The forces and the simplified formulas are briefly introduced in the following subsections and are applied in the contact model.

4.2.1 Stokes drag force

For a sphere of radius, a, with a steady velocity, U, moving through an incompressible fluid with viscosity, μ, when the Reynolds number is small, Stokes (1880) derived a drag force as $\tilde{f}_D = 6\pi a\mu U$. From experimental results for Reynolds number greater than one, a coefficient, $\phi(Re)$, is multiplied as a correction factor to account for the inertia effect. Hence, the drag force is computed as:

$$\tilde{f}_D = 6\pi a\mu U\phi(Re) \tag{4.1}$$

with

$$\phi(Re) = 1 + 0.15Re^{0.687} \tag{4.2}$$

for $1 < Re < 800$; a complete list of $\phi(Re)$ for a sphere over a range of Reynolds numbers can be found in Clift *et al.* (1978).

When a sphere moves close to a wall, the existence of the second boundary restricts the evolution of the fluid flow surrounding the sphere. Brenner (1961) developed a correction term for Stokes drag by solving the quasi-steady Stokes equation; the viscous drag force is represented as $\tilde{f}_D = 6\pi a\mu U\lambda(\delta^*)$, where $\delta^* = h/a$ is the non-dimensional gap scaled by the radius of the sphere. A '*' mark is used to distinguish from the previous non-dimensional gap $\delta = h/D$ scaled by the diameter. The value of $\lambda(\delta^*)$ increases with diminishing gap and converges to the classical lubrication theory when $\delta^* = 0$.

For flow at higher Reynolds number, the convective acceleration of the liquid between the two solid boundaries becomes important and a small gap Reynolds number, $Re_h = hU/\nu$, is defined. Cox & Brenner (1967) extended the correction term and incorporated the gap Reynolds number as:

$$\lambda(\delta^*, Re_h) = \frac{1}{\delta^*}\left[1 + \frac{1}{5}(1 \pm \frac{1}{4}Re_h)\delta^* \log\frac{1}{\delta^*}\right] \tag{4.3}$$

where a plus sign in front of the gap Reynolds number is used for an approaching sphere and a negative sign is used when the sphere rebounds from the wall. Then, the wall-modified viscous drag can be written as:

$$\tilde{f}_D = 6\pi a\mu U\lambda(\delta^*, Re_h). \tag{4.4}$$

Thus, for a sphere moving toward a solid wall, the drag force can be calculated by using equation (4.1) with (4.2) when it is far from the wall and equation (4.4) with correction term (4.3) when it is close to the wall. The transition is made at the position where two different correction terms converge to a single value.

4.2.2 Added mass force

Friedrich Bessel proposed the concept of added mass in 1828 to describe the motion of a pendulum in a fluid (see Stokes, 1851). The period of such a pendulum increased relative to its period in a

vacuum (even after accounting for buoyancy effects), indicating that the surrounding fluid increased the effective mass of the system. Added mass, also known as 'virtual' mass is the inertia added to a body because it must move some volume of surrounding fluid as it accelerates or decelerates since the body and fluid cannot occupy the same physical space simultaneously. A recent paper by Bagchi & Balachandar (2003) can be consulted for a detailed discussion.

To find the added mass force with the wall effect, the kinetic energy in the fluid phase when a solid sphere moves towards a wall at velocity $U(t)$ is calculated (see Milne-Thomson, 1968) as:

$$T = \frac{1}{4} m_l U^2(t) \left[1 + 3W(\delta^*)\right],$$

where $m_l = 4/3\pi a^3 \rho_l$ is the mass of the liquid displaced by the sphere and $W(\delta^*) = \sum_{n=1}^{\infty} \left(\frac{\mu_n}{\mu_0}\right)$. The infinite sum term results from a series of dipole images accounting for the wall in the upstream flow. The upstream flow is considered to be potential flow since the vorticity is confined to boundary layer for the particle Reynolds numbers beyond the Stokes flow regime. The functions μ_n with $n = 0, 1, \cdots$ depend on sphere center-to-wall distance $l = (\delta^* + 1)$.

When using the time rate of change of the total kinetic energy in the fluid phase as the work done by a moving sphere, the added mass force can be calculated as:

$$\tilde{f}_{AM} = -\frac{1}{U}\frac{dT}{dt} = -\frac{1}{2} m_l \frac{dU}{dt} - \frac{3}{2} m_l W(\delta^*) \frac{dU}{dt} - \frac{3}{4} m_l U \frac{dW(\delta^*)}{dt}. \tag{4.5}$$

The first term involving dU/dt on the right hand side is the conventional added mass term for a sphere moving in an unbounded flow. The last two terms account for the wall effect. With the relation $dW(\delta^*)/dt = (dW/d\delta^*)(d\delta^*/dt)$ and $d\delta^*/dt = (1/a)dh/dt = -U/a$, the third term can be written as $(3/4)m_l(U^2/a)(dW/d\delta^*)$.

Yang (2006) analyzed the expression of the wall correction terms in detail and approximated the infinite sum with a finite sum. After compared with experimental results from a pendulum collision,

Yang presented $W(\delta^*)$ in the second term of equation (4.8) and $dW/d\delta^*$ in the third term as:

$$W_7(\delta^*) = \frac{1}{8l^3} + \frac{1}{(4l^2-1)^3} + \frac{1}{(8l^3-4l)^3} + \frac{1}{(16l^4-12l^2+1)^3} + \frac{1}{(32l^5-32l^3+6l)^3} + \frac{1}{(64l^6-80l^4+24l^2-1)^3} + \frac{1}{(128l^7-192l^5+80l^3-8l)^3}; \tag{4.6}$$

$$\frac{dW}{d\delta^*} = \begin{cases} \dfrac{1}{128l^2(l^2-1)(2l^2-1)^3} - \dfrac{3l(4l^2-3)}{2(l^2-1)(4l^2-1)^4} + \dfrac{l}{2(l^2-1)(4l^2-1)^3} \\ \quad - \dfrac{8l^4-8l^2+1}{128l^4(l^2-1)(2l^2-1)^4} + \dfrac{1}{16l^2(l^2-1)} - \dfrac{2l^2-1}{16l^4(l^2-1)} & \text{for } l > 2; \\ 0.24 - \frac{2.3\times10^{-4}}{\delta^{*1/2}} - 0.31\delta^{*1/2} + 0.066\delta^* + 0.098\log\delta^* - \frac{2.06\times10^{-4}\log\delta^*}{\delta^{*1/2}} & \text{for } l \le 2 \end{cases} \tag{4.7}$$

where $l = \delta^* + 1$ is the non-dimensionalized sphere center-to-wall distance.

Then, the added mass force exerted on the sphere as it approaches to a wall can be calculated as

$$\tilde{f}_{AM} = -\frac{1}{2}m_l\frac{dU}{dt} - \frac{3}{2}m_l W(\delta^*)\frac{dU}{dt} + \frac{3}{4}m_l\frac{U^2}{a}\frac{dW(\delta^*)}{d\delta^*}. \tag{4.8}$$

with the wall effect terms defined in equations (4.6) and (4.7).

4.2.3 History force

The history force, also known as Basset force, describes the force due to the lagging boundary layer development with changing relative velocity (acceleration or deceleration) of a body moving through a viscous fluid (see Crowe *et al.*, 1998*b*). It is a direct consequence of non-constant vorticity generation at an unsteady solid surface, which affects the boundary layer development as compared to the growth on a surface moving with constant velocity. The varying boundary layer interacts with the unsteady surface motion resulting in a viscous force that is not accounted for by a quasi-steady drag. The history force is difficult to implement and is commonly neglected for practical reasons; however, it can be substantially larger than the added mass force when the body is accelerated at a high rate.

After solving the creeping flow with a low Reynolds number, Boussinesq (1885) and Basset (1888)

found the total hydrodynamic force for a sphere moving with velocity $U(t)$ in an unbounded viscous liquid as:

$$f = -6\pi\mu a U(t) - \frac{1}{2} m_l \frac{dU}{dt} - 6\pi\mu a^2 \frac{1}{\sqrt{\pi\nu}} \int_0^t \frac{dU}{d\tau} \frac{d\tau}{\sqrt{t-\tau}}. \tag{4.9}$$

where the first two terms are the steady drag force and the added mass force. The third term is the history force, which is calculated as a time integral that depends on the acceleration history of the sphere and a time kernel $K(t-\tau) = (t-\tau)^{-1/2}$. The time kernel describes the local dissipation mechanism and diminishes the effect of the history force due to the earlier sphere acceleration. Coimbra *et al.* (2004) confirmed the decay rate 1/2 for Stokes flows by their experiments involving an oscillating flow over a stationary sphere in which the flow unsteadiness was limited to high frequency and small amplitude.

To extend the history force for a moderate Reynolds number flow, numerical simulations were performed to investigate the unsteady hydrodynamic forces on a solid sphere. When preserving the forms of drag force and the added mass force, Mei & Adrian (1992) developed a new time kernel $K_{MA}(t-\tau, Re)$ for the history force through regular perturbation with low frequency. The term $K_{MA}(t-\tau, Re)$ has a form in which a faster decay as $(t-\tau)^{-2}$ is dominant when the Reynolds number is higher. Thus the history force has a shorter memory of flow disturbance at early times, as compared to $(t-\tau)^{-1/2}$ for low Reynolds number.

Kim, Elghobashi & Sirignano (1998) further extended Mei and Adrian's results by including unsteadiness from low to high frequencies and small to large amplitudes. A new time kernel is proposed as

$$K(t-\tau, Re) = \left\{ \left[\frac{\pi(t-\tau)\nu}{a^2} \right]^{1/2C_1} + G(\tau) \left[\frac{\pi |U(t)|^3 (t-\tau)^2}{2a\nu g_H^3(Re)} \right]^{1/C_1} \right\}^{-C_1} \tag{4.10}$$

where $g_H(Re) = 0.75 + C_2 Re$ is a fitted function, $C_1 = 2.5$ and $C_2 = 0.126$. $G(\tau)$ is a weight function of the primary and the secondary flow acceleration number, with $M_1(\tau) = (2a/U^2)|dU/d\tau|$ and $M_2(\tau) = (2a^2/|U^3|)|d^2U/d\tau|^2$, as $G(\tau) = 1/\left[1 + \beta(\tau)\sqrt{M_1(\tau)}\right]$. A second fitted function, $\beta(\tau) = C_5/\{1 + \phi_r^{1+C_4}/[C_3(\phi_r + \phi_r^{C_4})]\}$, depends on the acceleration ratio, $\phi_r(\tau) = M_2(\tau)/M_1(\tau)$

with $C_3 = 0.07$, $C_4 = 0.25$, $C_5 = 22.0$. This time kernel covers both of the previous results for creeping flow and for moderate Reynolds number flow with a complete range of oscillating conditions.

As summarized by Yang (2006), various history kernels have been proposed that focus on the long-time behavior of the history force beside the above citations. Different velocity variations, including an impulsive start or stop, constant acceleration, and a step velocity change, have been employed to evaluate the unsteady drag on a solid body (see Hinch, 1993; Lovalenti & Brady, 1993; Lawrence & Mei, 1995; Chaplin, 1999). The history kernels for the different flows have different forms: $K(t-\tau) \sim e^{-(t-\tau)}$, $(t-\tau)^{-n}$, or $(t-\tau)^{-n}e^{-(t-\tau)}$ with $n > 1/2$. However, experimental result that can validate the long-term history force behavior is absent.

The influence of the existence of a solid wall on the history force exerted on a moving sphere was investigated by Yang (2006) based on a similar technique as used for the added mass force. Based on a wall-modified potential function, a modified history force different from the no-wall results was formulated by examining the effect of the potential pressure field on the boundary layer development as:

$$\tilde{f}_H = -6\pi\mu a K_H(\delta^*)^{3/2} \int_0^t \frac{dU}{d\tau} K(t-\tau) d\tau \tag{4.11}$$

where $K_H(\delta^*)$ is the the wall-effect factor and it has a form with $l = \delta^* + 1$ as

$$\begin{aligned} K_H(\delta^*) = 1 + \frac{0.375 - 0.03125/(1-2l^2)^3}{l^3} - \frac{3}{(1-4l^2)^3} - \frac{0.015625}{(l-2l^3)^3} \\ + \frac{1}{(1-12l^2+16l^4)^3} + \frac{0.375}{(3l-16l^3+16l^5)^3}. \end{aligned} \tag{4.12}$$

The argumentation factor, to the order of l^{-15}, is found to increase monotonically with diminishing δ^*.

Yang (2006) did pendulum-wall collision experiments and validated the history force with the wall-modified factor (4.12) and also the kernel (4.10). For a particle-wall collision process, a short-term characterization of $\tilde{f}_H$ is more important. Thus, the expression (4.11) with (4.10) and (4.12) is used to calculate the history force exerted on a sphere in the following contact model.

4.2.4 Liquid-solid force term in the contact model

The formulas for the hydrodynamic forces exerted on a sphere moving in a liquid environment developed by Yang (2006) provide a direct and simple source for modeling the liquid-solid interaction force in a numerical simulation for a sphere-wall collision process when the sphere is close to the wall and the resolution is insufficient.

As a first step, the computed results obtained from a numerical simulation for a sphere falling toward a wall under gravity are compared with the results calculated from the theoretical expressions developed by Yang (2006). To obtain the simulated and analytical results, the experimental results from the current experiments described in chapter 2 are used. Sixth order polynomial curves are employed to fit the measured trajectories so that the velocity and acceleration of the sphere at different times can be calculated by differentiating the polynomial. The fitting curves are used to prescribe the motion of the sphere in the numerical simulation. The force obtained from the simulation is still marked as $\tilde{f}_{\text{SIM}}$. For the analytical results, the total hydrodynamic force is calculated as:

$$\tilde{f}_{\text{THR}} = \tilde{f}_D + \tilde{f}_{AM} + \tilde{f}_H \tag{4.13}$$

where $\tilde{f}_D$ is the Stokes drag force calculated from equation (4.1) and (4.4) with the wall correction term (4.3); the added mass force $\tilde{f}_{AM}$ is calculated from equation (4.8) with the wall correction terms (4.6) and (4.7); the history force $\tilde{f}_H$ is calculated from equation (4.11) with the wall correction term (4.12) and the time kernel (4.10). The smooth velocity and acceleration profiles calculated by differentiating the polynomial fitting curves are used in the equations mentioned above. After performing the numerical simulations and the corresponding calculations, the comparison shows that the simulated force matches with the theoretical result well at moderate gap and there is no deviation until the gap becomes small.

As an example, for a sphere moving with a prescribed trajectory obtained from the experimental case 3 with particle impact Reynolds number $Re = 90$, the hydrodynamic forces are plotted as a function of the non-dimensional gap between the sphere and the wall, $\delta = h/D$, as well as its wall

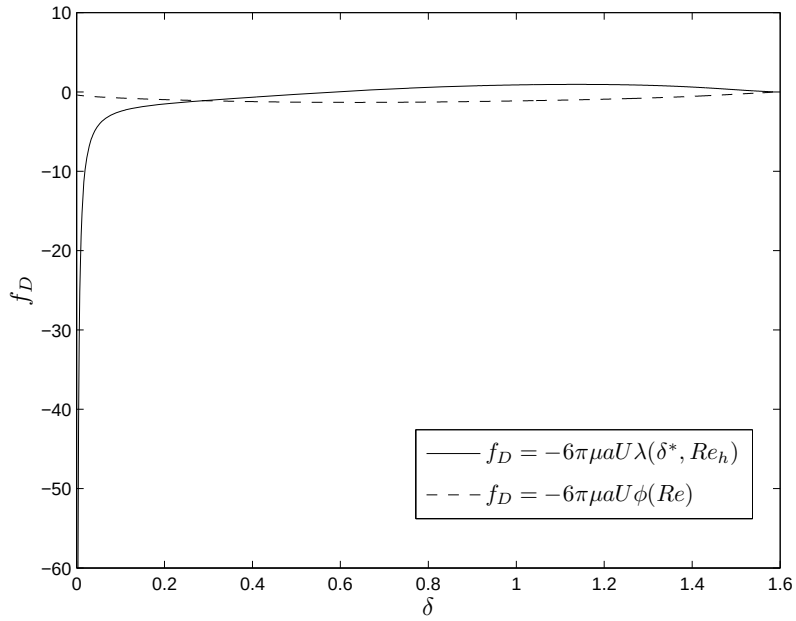

Figure 4.2: The Stokes drag as a function of the gap

correction coefficient.

The Stokes drag forces calculated with the Reynolds number correction and the wall correction are shown in figure (4.2) respectively as solid line and dashed line. The force is non-dimensionalized by $\frac{4}{3}\pi a^3\rho_l g$ and denoted as f_D without the hat tilde. The same non-dimensionalization is performed for all the other forces. The wall correction term for the Stokes drag force, $\lambda(\delta^*, Re_h)$, is plotted in figure (4.3). When the gap is large ($\delta > 0.6$), the calculated result is negative, which is not correct since equation (4.3) is for small gap. As shown in figure (4.2), the results obtained from the two different formulas have a matching range around $\delta = 0.3$ so that the value calculated with the Reynolds number correction is used for $\delta > 0.3$ and the value calculated with the wall correction is used for $\delta < 0.3$. The magnitude of the drag force increases dramatically with the diminishing gap. It plays a dominant role in the hydrodynamic forces exerted on the sphere when it is about to collide with a wall.

Similarly, the non-dimensional added mass force f_{AM} and its wall correction terms $W(\delta^*)$ and $dW(\delta^*)/d\delta^*$ are plotted as a function of the gap as shown in figure (4.4) and (4.5). The non-

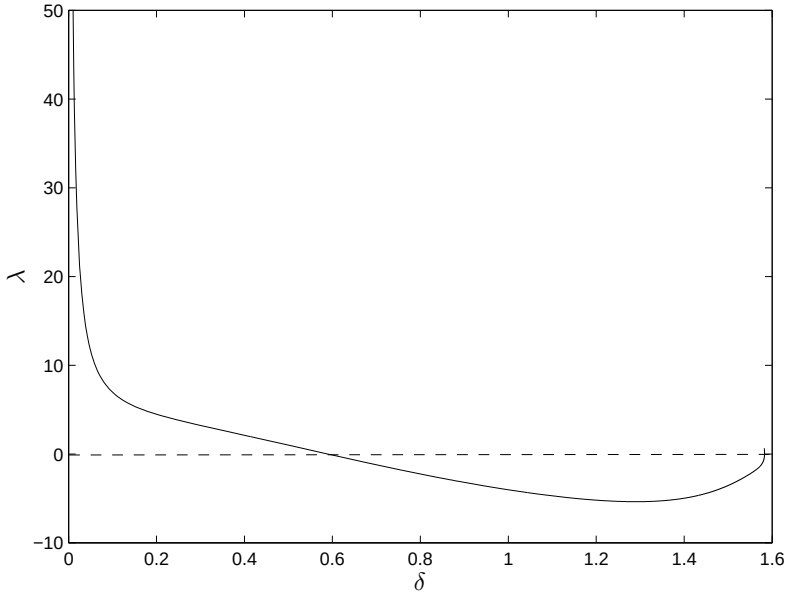

Figure 4.3: Wall correction term for Stokes drag as a function of the gap

dimensional history force f_H and its wall correction term $K_H(\delta^*)$ are plotted in figure (4.6) and (4.7).

After comparing the results in figure (4.2), (4.4) and (4.6), the magnitude of the added mass force and the history force are smaller than the Stokes drag force when the sphere is approaching to the wall. The total force effect as $f_{\text{THR}} = f_D + f_{AM} + f_H$ when the sphere is close to the wall is plotted as a dashed line in figure (4.8).

In the same figure, the simulated result obtained from a numerical simulation by prescribing the motion of the sphere with the measured trajectory from the experiment case 3 is plotted as a solid line. The two results match well when the gap is moderate. The results deviate when the gap is less than 0.1 and there is insufficient resolution in the numerical simulation.

To resolve the flow when the gap is small, a liquid-solid interaction model is proposed that blends the simulated and the theoretical forces whenever the gap decreases below a threshold value, δ_{SL}. The solid-liquid force, $\tilde{f}_{\text{SL}}$ is obtained as

$$\tilde{f}_{\text{SL}} = H\left(\frac{\delta}{\delta_{\text{SL}}}\right)\tilde{f}_{\text{THR}} + [1 - H\left(\frac{\delta}{\delta_{\text{SL}}}\right)]\tilde{f}_{\text{SIM}}, \tag{4.14}$$

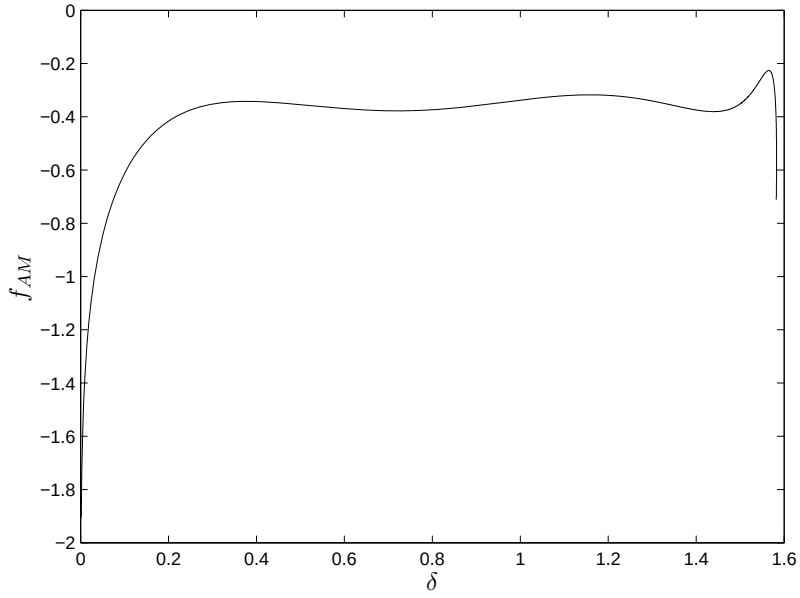

Figure 4.4: The added mass force as a function of the gap

where

$$H\left(\frac{\delta}{\delta_{\text{SL}}}\right) = \frac{1}{1+e^{10\left(\frac{\delta}{\delta_{\text{SL}}}-1\right)}} \tag{4.15}$$

is a smoothed Heaviside function, as shown in figure (4.9). Based on figure (4.8), δ_{SL} is conservatively taken as 0.2. Clearly, the necessary value of δ_{SL} depends on the grid resolution of the fluid simulation. The finer the grid, the smaller the value of δ_{SL} that could be used. On the other hand, it seems reasonable to fix the value at a conservative value independent of the grid resolution.

Thus, for a sphere approaching a wall, the hydrodynamic force exerted on it is computed directly from the simulation when the distance between the sphere and the wall is large ($\delta > 0.4$); the analytical results start to be counted in when $\delta < 0.4$ and the hydrodynamic force has a form:

$$\tilde{f}_{\text{SL}} = \frac{1}{2}\tilde{f}_{\text{THR}} + \frac{1}{2}\tilde{f}_{\text{SIM}}$$

at $\delta = 0.2$; when the sphere is about to collide with the wall, the hydrodynamic forces are taken as the values calculated from the analytical expressions as the gap decreases to zero.

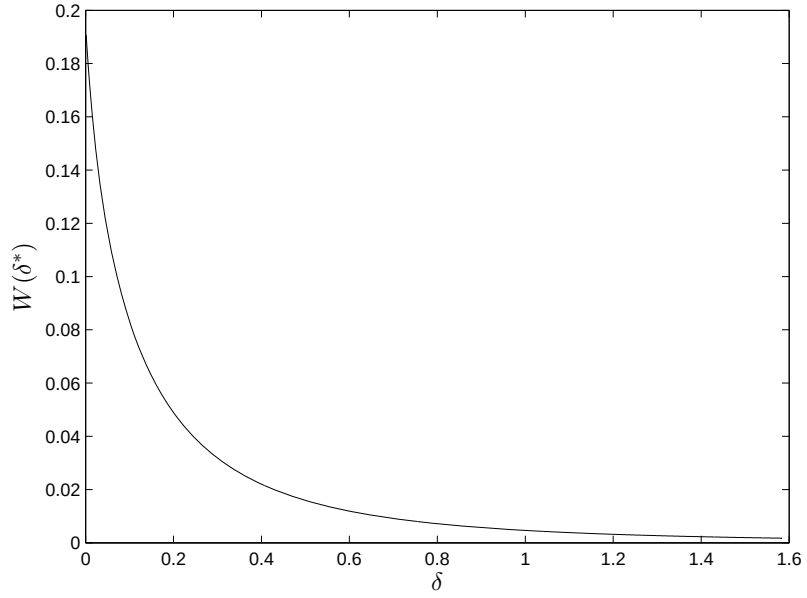

(a)

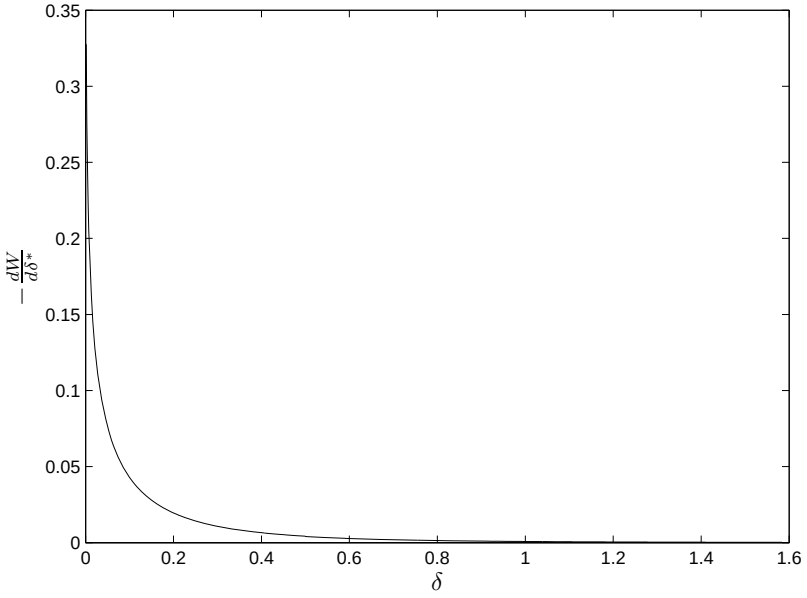

(b)

Figure 4.5: The wall correction term for added mass as a function of the gap

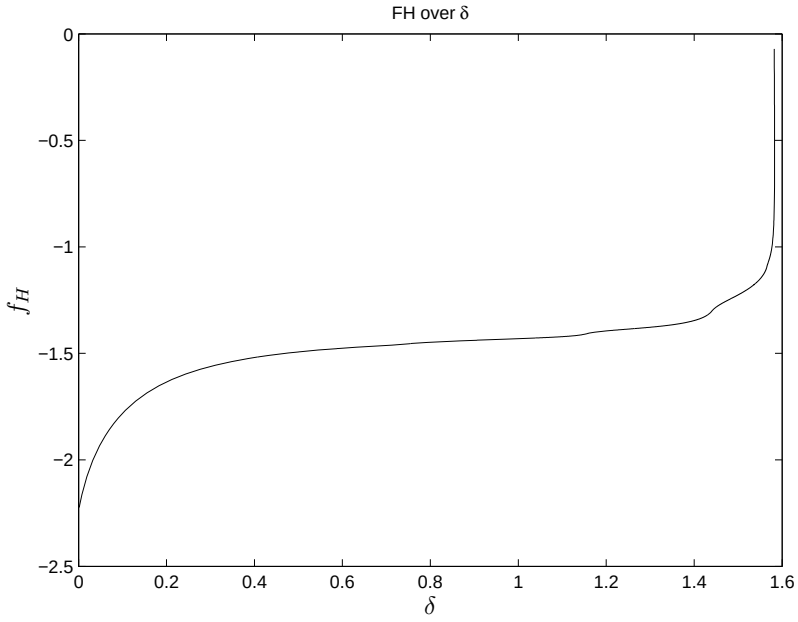

Figure 4.6: The history force as a function of the gap

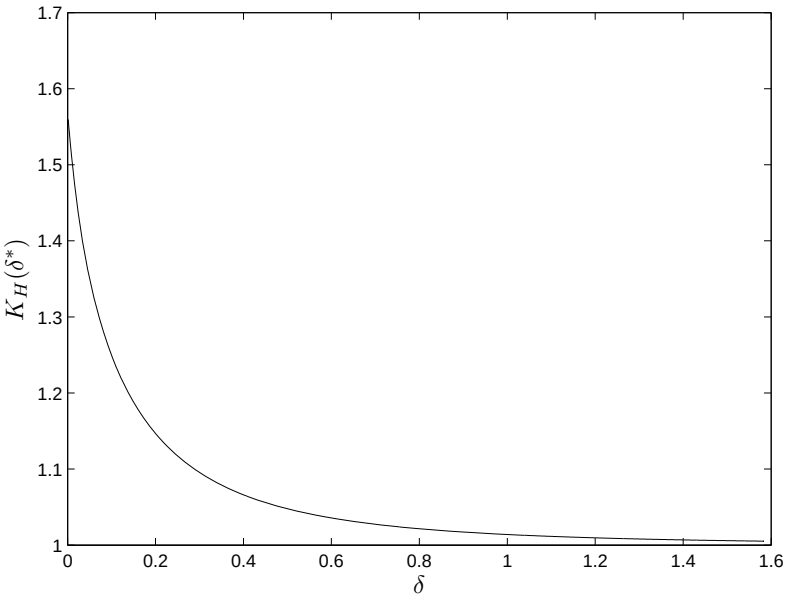

Figure 4.7: The wall correction term for history force as a function of the gap

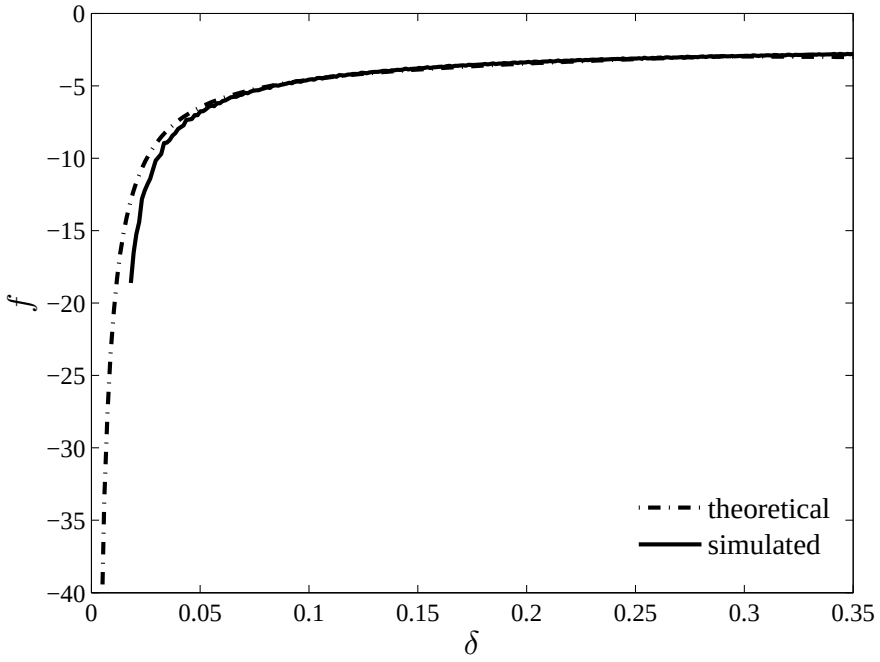

Figure 4.8: The liquid-solid interaction force for a impact process with $Re = 90$.

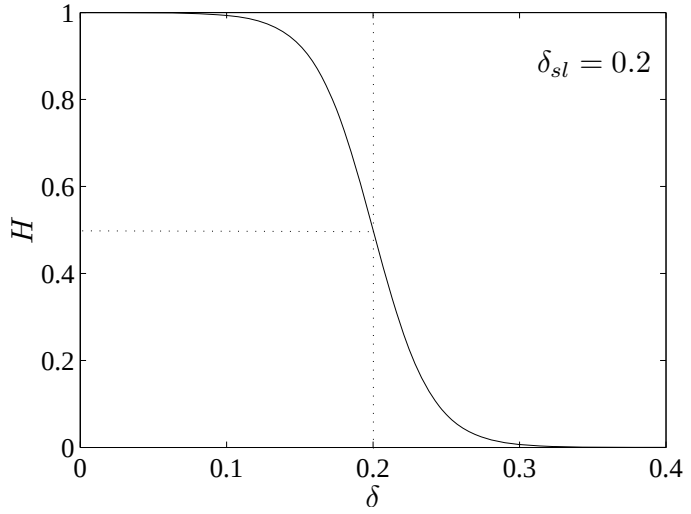

Figure 4.9: The smooth Heaviside function H for $\delta_{\mathrm{SL}} = 0.2$.

4.3 Elastic effect of the solid parts

The hydrodynamic forces discussed in section 4.2 increase rapidly as a sphere approaches a wall and dissipate the kinetic energy of the system. At an extreme, the velocity decreases to zero so that the sphere stops and rests on the wall, as shown in the settling experiments in chapter 2. However, part of the kinetic energy is stored when the incoming velocity is large and the sphere has more inertia. This kinetic energy is transformed into elastic-strain energy so that the sphere deforms and rebound may occur.

In elastohydrodynamic theory, the two deformable solid surfaces are assumed to be smooth and to be separated by a thin incompressible Newtonian fluid layer that prevents the surfaces from actually touching. A large hydrodynamic pressure builds up as the fluid is squeezed out from the gap between the sphere and the wall and causes the elastic solid to deform. Davis, Serayssol & Hinch (1986) first simultaneously accounted for elastic formation and viscous fluid forces by describing the deformation of the sphere following the development of Hertz contact theory of linear elasticity. Lubrication theory is employed to couple the deformation geometry with the pressure profile of the interstitial liquid. They were not able to obtain the analytical solution for the dynamic deformation and viscous forces. Wells (1993) and Lian, Adams & Thornton (1996) proposed their more simplified models where the dynamic deformation of the spheres was assumed to be Hertzian-like and presented approximate analytical solutions for the evolution of the relative particle velocity, force and restitution coefficient.

In the current work, the coupling between the elastic solid mechanics and fluid dynamics is interpreted in another way. The hydrodynamic force building up in the interstitial fluid is incorporated in the liquid-liquid interaction term $\tilde{f}_{\mathrm{SL}}$ since the analytical expressions with the wall correction terms converge to the lubrication theory with diminishing gap between the sphere and the wall. The deformation of the solid surfaces are not included in the numerical simulations. However, the conversion between the kinetic energy and the elastic-strain energy is represented by adding an additional term into the equation of the sphere motion based on the Hertz contact theory. When the gap between the two solid surfaces decreases below a threshold value, the solid elastic term starts to take effect

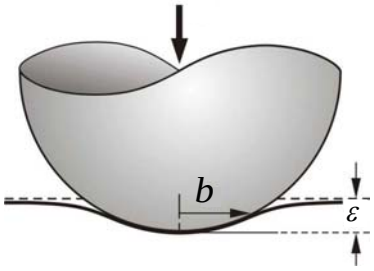

Figure 4.10: Schematic of a contact between a sphere and an elastic half space.

decreasing the impacting velocity and making the sphere rebound.

4.3.1 Hertz contact theory

Hertz contact theory investigates the local stresses that develop as two curved surfaces come into contact and deform slightly under an imposed load. It is named after Heinrich Hertz, who initiated the study of the deformation of solids that touch each other (see Hertz, 1882) and provided many important ideas for the development of contact mechanics.

For an elastic sphere with radius a indenting an elastic half-space to depth ε, with a contact area of radius b, as shown in figure (4.10), the contact force calculated from the Hertz contact theory (see Johnson, 1985) is:

$$W = \frac{4}{3} E^* a^{1/2} \varepsilon^{3/2} \tag{4.16}$$

where $E^* = [(1-\nu_1^2)/E_1 + (1-\nu_2^2)/E_2]^{-1}$ is the reduced modulus based on the Young's Modulus, E, and the Poisson ratio, ν, for the two materials. The indentation depth ε is related to the impacting velocity as $V = \frac{d\varepsilon}{dt}$. The equation of motion of the sphere can be described as:

$$m_p \frac{d^2\varepsilon}{dt^2} = -\frac{4}{3} E^* \sqrt{a} \varepsilon^{3/2} \tag{4.17}$$

Solving this equation with an initial condition $\frac{d\varepsilon}{dt} = V_I$ when $\varepsilon = 0$ yields:

$$\frac{d\varepsilon}{dt} = \sqrt{V_I^2 - \frac{16 E^* \sqrt{a}}{15 m_p} \varepsilon^{5/2}}$$

At the end of the elastic deformation process, the maximum depth is given when $V = \frac{d\varepsilon}{dt} = 0$. So:

$$\varepsilon_{\max} = \left(\frac{15 m_p V_I^2}{16 E^* \sqrt{a}}\right)^{2/5}$$

Thus, the maximum elastic force for a spheres with an impacting velocity V_I is:

$$W_o = \frac{4}{3} E^* \sqrt{a} \left(\frac{15 m_p V_I^2}{16 E^* \sqrt{a}}\right)^{3/5}$$

which can be simplified by applying $m_p = 4/3\pi a^3 \rho_p$ into:

$$W_o = \frac{4}{3} a^2 E^* \left(\frac{5\pi}{4E^*} \rho_p V_I^2\right)^{3/5} \tag{4.18}$$

4.3.2 Elastic effect term in the equation of motion

Based on the expression (4.18) of the maximum Hertz elastic force achieved during a collision process for an elastic sphere and an elastic wall, an elastic force is proposed for the contact model as:

$$\tilde{f}_{\text{ss}} = F\left(\frac{\delta}{\delta_{\text{ss}}}\right) e_d W_o, \tag{4.19}$$

where the subindex $_{\text{ss}}$ indicates the elastic force results from the approaching of the two solid surfaces. The dry coefficient of restitution e_d is taken as 0.97 as mentioned in Chapter 1, which incorporates the inelasticity. The function $F\left(\frac{\delta}{\delta_{\text{ss}}}\right)$ is used to introduce the elastic effect gradually after the gap between the sphere and the wall decreases below a threshold value, δ_{ss}; W_o is the maximum elastic force calculated from equation (4.18) where the impact velocity V_I is taken to be the value when $\delta = \delta_{\text{ss}}$. Different forms of the function $F\left(\frac{\delta}{\delta_{\text{ss}}}\right)$ have been tried and the one that produces the best fit for the particle trajectory has the following form:

$$F\left(\frac{\delta}{\delta_{\text{ss}}}\right) = \begin{cases} \frac{e^{\left(-\frac{\delta}{\delta_{\text{ss}}}\right)} - e^{-1}}{1 - e^{-1}}, & 0 \le \delta \le \delta_{\text{ss}}; \\ 0, & \delta > \delta_{\text{ss}}. \end{cases} \tag{4.20}$$

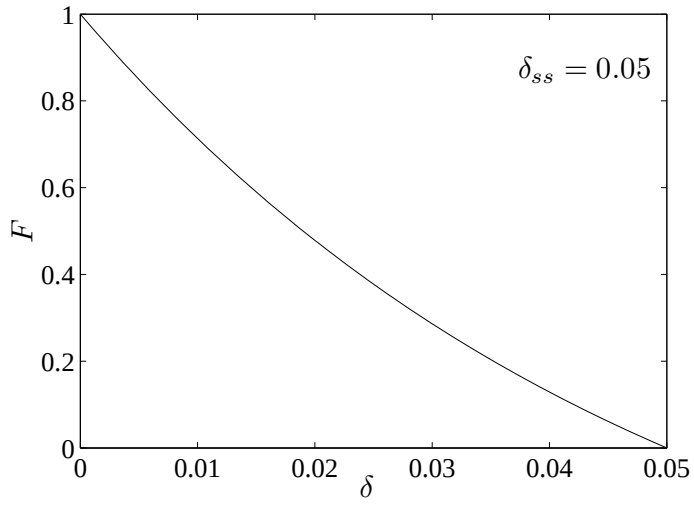

Figure 4.11: F function for $\delta_{\text{ss}} = 0.05$

The dependence of F on the gap is plotted in figure (4.11).

Thus, when the gap is large, there is no elastic effect on the sphere; however, when the gap decreases and approaches zero, the elastic effect increases and approaches the maximum elastic force achieved in a dry collision. This additional elastic force term converts the kinetic energy of the impacting sphere and make it rebound. The non-dimensional parameter δ_{ss}, is the threshold where the elastic force starts to take effect and it plays an important role in the contact model. The choice of the value and physical meaning of δ_{ss} will be discussed in detail in Chapter 5.

At distance $\delta < \delta_{\text{ss}}$, the velocity of the impacting sphere decreases dramatically due to the elastic force and becomes zero when the gap between the sphere and the wall reaches a minimum value. The velocity of the sphere keeps decreasing to negative (opposite direction) value so that the sphere rebounds under the elastic effect until the growing gap exceeds the threshold value δ_{ss}.

4.4 Contact model for normal sphere-wall collisions

After including the liquid-solid interaction force term and the elastic effect term, the final equation of the motion in the vertical direction with the contact model is written as:

$$m_p \frac{d\tilde{V}}{d\tilde{t}} = \tilde{f}_{\text{SL}} + \tilde{f}_{\text{SS}} + m_p g + \tilde{f}_b, \tag{4.21}$$

It can be non-dimensionalized after applying the same characteristic length $L_o = D$ and time $t_o = \sqrt{D/g}$:

$$\tau \frac{dV}{dt} = f_{\text{SL}} + f_{\text{SS}} + \tau - 1, \tag{4.22}$$

where $\tau = \rho_p/\rho_l$ is the density ratio, f_{SL} and f_{SS} are the non-dimensional liquid-solid interaction and elastic forces. After coupling the equation (4.22) with the evolution of the flow field:

$$\frac{\partial \mathbf{u}}{\partial t} + \mathbf{u} \cdot \nabla \mathbf{u} = -\nabla p + \frac{1}{Re} \nabla^2 \mathbf{u} + \int_s \mathbf{f}(\boldsymbol{\xi}(s,t)) \delta(\boldsymbol{\xi} - \mathbf{x}) ds$$

and the boundary condition:

$$r\boldsymbol{u}(\boldsymbol{\xi}(s,t)) = \int_{\boldsymbol{x}} r\boldsymbol{u}(\boldsymbol{x}) \delta(\boldsymbol{x} - \boldsymbol{\xi}) d\boldsymbol{x} = r_B \boldsymbol{u}_B(\boldsymbol{\xi}(s,t)),$$

both the motion of the sphere before and after the collision process can be computed with known input parameters based on the initial distance, the gravitational acceleration, the solid-liquid density ratio, the diameter of the sphere, and the viscosity of the liquid.